Static Pressure and Velocity Profiles in Swirling Incompressible Tube Flow

M. K. KING, R. R. ROTHFUS, and R. I. KERMODE

Carnegie Mellon University, Pittsburgh, Pennsylvania

The phenomenon of reversing axial flow in swirling incompressible flow through a tube has been investigated experimentally. The study was carried out in a 2 in. I.D. test section of plexiglass tubing 10 ft. long. The swirl was introduced by injection of the total fluid stream through two symmetric tangential inlets perpendicular to the tube. Measurements have been made with specially constructed stagnation and static pressure probes.

Velocity and pressure profiles obtained for tests conducted at four Reynold's Numbers in one fixed geometrical configuration are presented and discussed in general terms. Swirl decay rate is characterized in a plot of weighted tangential velocity/inlet velocity ratio versus distance along the test section from the inlets. A model presented by a previous investigator to explain the flow reversal phenomenon is discussed in the light of present work. Finally the data is used in an order of magnitude analysis to reduce the turbulent Navier-Stokes equation describing the flow to simpler (though still indeterminate) form.

In recent years, a large number of experimental and analytical studies covering many classes of swirling flows have been conducted. These studies may be arbitrarily divided into three rough classifications:

1. Unconfined swirling flows (including swirling flows within boundaries where wall effects may be neglected). Flows falling into this category include rotary gas burner flows, trailing vortices from aircraft wings, swirling free jets, and swirling compressible nozzle flows where boundary layer effects are negligible.
2. Swirling flows in short, large diameter chambers where end-wall effects interact with the swirl flow to produce strong secondary flow effects. (Studies of the gaseous nuclear rocket swirling flow core containment concept have made up the bulk of work in this area.)
3. Swirling flows in large L/D tubes where circumferential wall effects interact strongly with the vortex flow. The work reported in this paper falls into this third category.

Considerable study of swirling compressible flow in tubes (the Ranque-Hilsch tube) has been carried out since 1950 (*5, 8, 12* to *14*). However, relatively little work in the area of swirling incompressible tube flow is to be found in the literature; the bulk of the compressible flow work has been aimed mainly at characterizing and understanding the ability of the Ranque-Hilsch tube to produce temperature separation, rather than investigating the phenomenon of axial flow reversal in swirling tube flows (the purpose of this study).

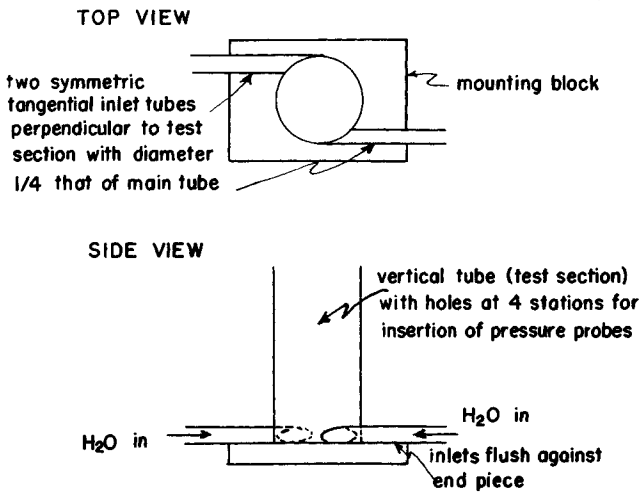

Fig. 1. Test section used by Bresan to study swirling flow.

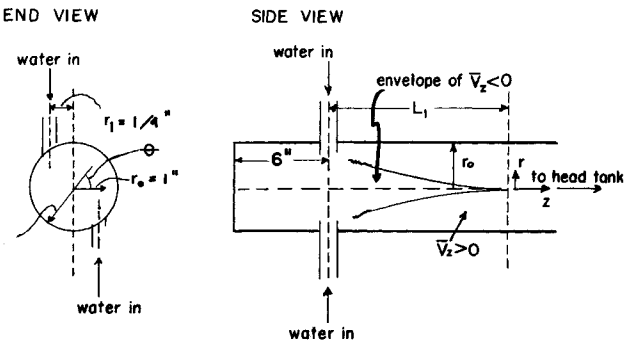

Fig. 2. Test section used in this study of swirling flow.

In studies of swirling incompressible tube flow conducted by Peck (*11*) and Beal (*1*), dye injection was used to identify a region of reversed axial flow near the centerline of the tube. Binnie (*3*) and Nettall (*10*) likewise noted axial flow reversal in swirling incompressible pipe flows, along with the existence of a third flow regime. Under the most extreme swirl conditions, they found that the axial flow was normal (downstream) at the center of the tube and at the wall, but reversed in an intermediate region.

Kreith and Sonju (*7*) studied the decay of a liquid turbulent swirl which was induced by twisted metal strips along the centerline of a tube and correlated their results with a linearized model. In this work, the swirl was not sufficiently strong to produce flow reversal. Talbot (*15*) examined aqueous laminar swirling pipe flow experimentally and by linearized perturbation analysis. Again, the swirl strength was insufficient to produce flow reversal, but a dimpling of the axial velocity profile at the center of the tube was predicted and observed.

Bresan (*4, 9*) studied the swirling incompressible flow of water in a tube, with the swirl induced by tangential injection of the water into the test section as shown in Figure 1. In this study, he obtained static pressure and velocity profiles and developed a simple model for predicting axial flow reversal as a function of the swirl strength and decay rate.

In this investigation, a system somewhat similar to that of Bresan's was studied. A back-mixing region was added to the system (Figure 2) and an improved probe technique was used to determine pressure and velocity profiles. These profiles were determined for test section axial flow Reynold's numbers of 10,000, 15,000, 20,000 and 25,000.

M. K. King is with Atlantic Research Corporation, Alexandria, Virginia and R. I. Kermode is at the University of Kentucky, Lexington, Kentucky.

Under the assumption of axisymmetric flow (which was verified experimentally during the course of this study), the laminar Navier-Stokes equations for swirling tube flow may be written as

$$\rho\left(v_r\frac{\partial v_r}{\partial r}-\frac{v_\theta^2}{r}+v_z\frac{\partial v_r}{\partial z}\right)=-\frac{\partial p}{\partial r}+\mu\left(\frac{\partial^2 v_r}{\partial r^2}+\frac{1}{r}\frac{\partial v_r}{\partial r}-\frac{v_r}{r^2}+\frac{\partial^2 v_r}{\partial z^2}\right) \quad (1)$$

$$\rho\left(v_r\frac{\partial v_\theta}{\partial r}+\frac{v_\theta v_r}{r}+v_z\frac{\partial v_\theta}{\partial z}\right)=\mu\left(\frac{\partial^2 v_\theta}{\partial r^2}+\frac{1}{r}\frac{\partial v_\theta}{\partial r}-\frac{v_\theta}{r^2}+\frac{\partial^2 v_\theta}{\partial z^2}\right) \quad (2)$$

$$\rho\left(v_r\frac{\partial v_z}{\partial r}+v_z\frac{\partial v_z}{\partial z}\right)=-\frac{\partial p}{\partial z}+\mu\left(\frac{\partial^2 v_z}{\partial r^2}+\frac{1}{r}\frac{\partial v_z}{\partial r}+\frac{\partial^2 v_z}{\partial z^2}\right) \quad (3)$$

$$\frac{\partial v_r}{\partial r}+\frac{v_r}{r}+\frac{\partial v_z}{\partial z}=0 \text{ (continuity equation)} \quad (4)$$

However, since it was found necessary to operate in the turbulent flow regime to provide dynamic pressure high enough for detailed profile measurements, the following turbulent shear stress terms must be added to the right side of the laminar equations to make them applicable to the conditions studied:

$$z\text{-direction: } \frac{1}{r}\frac{\partial}{\partial r}(r\overline{\tau'_{rz}})+\frac{\partial\overline{\tau'_{zz}}}{\partial z}$$

$$\theta\text{-direction: } \frac{1}{r^2}\frac{\partial}{\partial r}(r^2\overline{\tau'_{r\theta}})+\frac{\partial\overline{\tau'_{\theta z}}}{\partial z}$$

$$r\text{-direction: } \frac{1}{r}\frac{\partial}{\partial r}(r\overline{\tau'_{rr}})-\frac{\overline{\tau'_{\theta\theta}}}{r}+\frac{\partial\overline{\tau'_{rz}}}{\partial z}$$

where $\overline{\tau_{ij}}' = -\rho\overline{v_i' v_j'}$.

The resulting set of turbulent Navier-Stokes equations is indeterminate by the six turbulent shear terms, $-\rho\overline{v_i' v_j'}$.

EXPERIMENTAL EQUIPMENT

A schematic diagram of the experimental equipment is shown in Figure 3. Two symmetric ½ in. diameter tangential inlets with equal flow rates were used to insure axisymmetric flow. These inlets introduced swirling flow into the 2 in. I. D., 120 in. long test section. Eight holes level with the test section centerline were spaced along the test section at 1 ft. intervals starting 18 in. downstream of the inlets to allow probing the flow field. To prevent excessive interaction of probes with the flow field, only one axial location at a time was probed, with the remaining holes being carefully sealed off.

Bresan's (*4*) results indicated that the time-averaged radial velocity component at any position more than 3 to 6 tube diam.

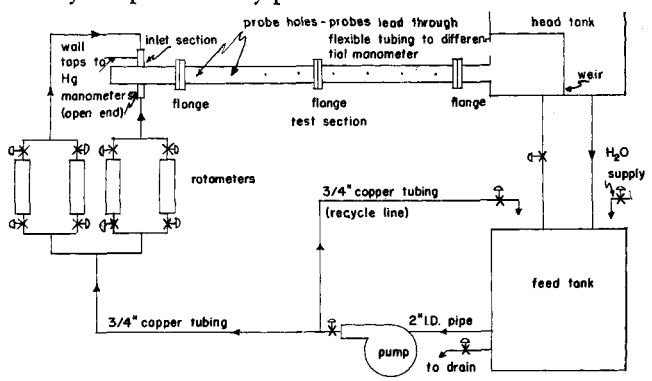

Fig. 3. Equipment schematic.

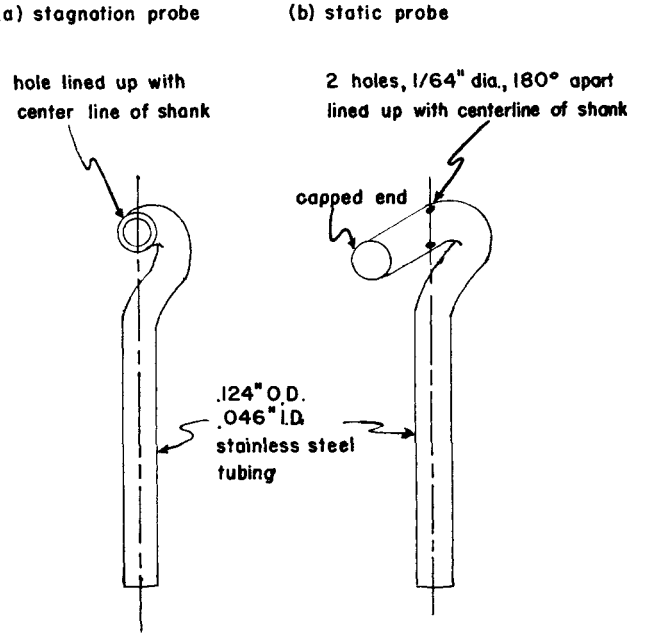

Fig. 4. Probes used in this study.

downstream of the inlet should be less than 1% of the resultant of the axial and tangential velocities. (This was verified during the course of this study from analysis of $\overline{v}_\theta$ and $\overline{v}_z$ profiles with use of the continuity equation.) Thus the system could be treated as a two-dimensional one with regard to probe design. Accordingly, separate static and stagnation probes which could be oriented into the axial-tangential resultant flow vector were designed. In this design, it was necessary to insure that the vertical position of the probe holes would not change with rotation of the probe in search of the proper orientation. (Variation of this vertical location would cause confusion of pressure reading changes caused by orientation of the velocity vector relative to probe orientation with changes in the head of water above the probe.) In addition, the holes in the static probe had to be placed so that they would pick up only the negligible radial velocity component. The resultant probe designs are shown in Figure 4.

A probe positioning jig permitted very accurate positioning of the probes with respect to distance from the tube centerline and orientation. (When we speak of orientation, we are referring to the rotation of the probe to point into the resultant of the tangential and axial velocity components.) The probes were calibrated in a one-dimensional flow system with proper orientation (probe pointing into the flow) and at various degrees of misorientation. The stagnation probe was found to be quite sensitive to orientation, yielding maximum readings at proper orientation and reading increasingly lower values with increasing degree of misorientation. This sensitivity permitted use of the stagnation probe for determination of flow angles in the test section (and thus for resolution of the resultant velocity into axial and tangential components).

A differential manometer, connected at one end to the probe being used and at the other to a shielded wall tap in the head tank level with the centerline of the test section, was used for measurement of pressure (static or stagnation) relative to pressure in essentially quiescent water at the same vertical position (reference pressure). (This procedure was necessary for nulling out the head of water in the collection tank which could easily vary from trial to trial depending on the height of the crest over the collection tank weir.)

EXPERIMENTAL PROCEDURE AND PRELIMINARY DATA REDUCTION

The step-by-step data taking procedure was as follows:

1. At the desired entry port (axial position) a traverse of the stagnation probe at zero flow was run to obtain zeroing readings on the differential manometer. These were later used to subtract out from test readings any discrepancies in the height of the probe relative to the height of the secondary tap caused by any slight probe jig misalignments.

2. Next the flow rate through the inlets was set to achieve

the desired $N_{Re0} = D_0 v_0 \rho/\mu$. The stagnation probe was set at a desired distance from the axis and readings taken at various orientation angles. These readings were plotted as a function of the angle to find the orientation which maximized the reading, giving the angle of flow. (Zero degrees was defined as the orientation with the probe facing the inlet end of the test section.) This procedure was repeated at other radial positions and Reynold's numbers.

3. Steps 1 and 2 were repeated at other ports (axial positions).

4. Steps 1, 2, and 3 were finally repeated with the static probe.

The first step in the data reduction was conversion of the measured static and stagnation pressures to dimensionless form. This step was necessary since static and stagnation pressure traverses were not all made at the same temperature. (Dimensional analysis shows that for a fixed geometry and a fixed N_{Re0}, the dimensionless quantities $\overline{P}_{stag}\ g_c/v_0^2$, $P_{static}\ g_c/v_0^2$, $\overline{v}_\theta/v_0$, and $\overline{v}_z/v_0$, are fixed as functions of dimensionless position, r/r_0 and z/r_0. Since, however, viscosity varies strongly with temperature, v_0 also varies with temperature at a fixed N_{Re0}. Thus, since the static and stagnation pressure traverses were not all run at the same temperature, v_0 was not always the same for measurements made at one fixed N_{Re0}. Therefore, $\overline{P}_{stat}$ and $\overline{P}_{stag}$ had to either be corrected to a common temperature or made dimensionless by conversion to $\overline{P}_{stat}\ g_c/v_0^2$ and $\overline{P}_{stag}\ g_c/v_0^2$ to be comparably meaningful and to permit resultant velocity calculations.)

Following conversion of the static and stagnation pressures to dimensionless form, $\overline{v}/v_0$ was calculated from

$$\overline{v}^2/v_0^2 = 2g_c\Delta\overline{p}/v_0^2 = 2(\overline{P}_{stag}\ g_c/v_0^2 - \overline{P}_{stat}\ g_c/v_0^2)$$

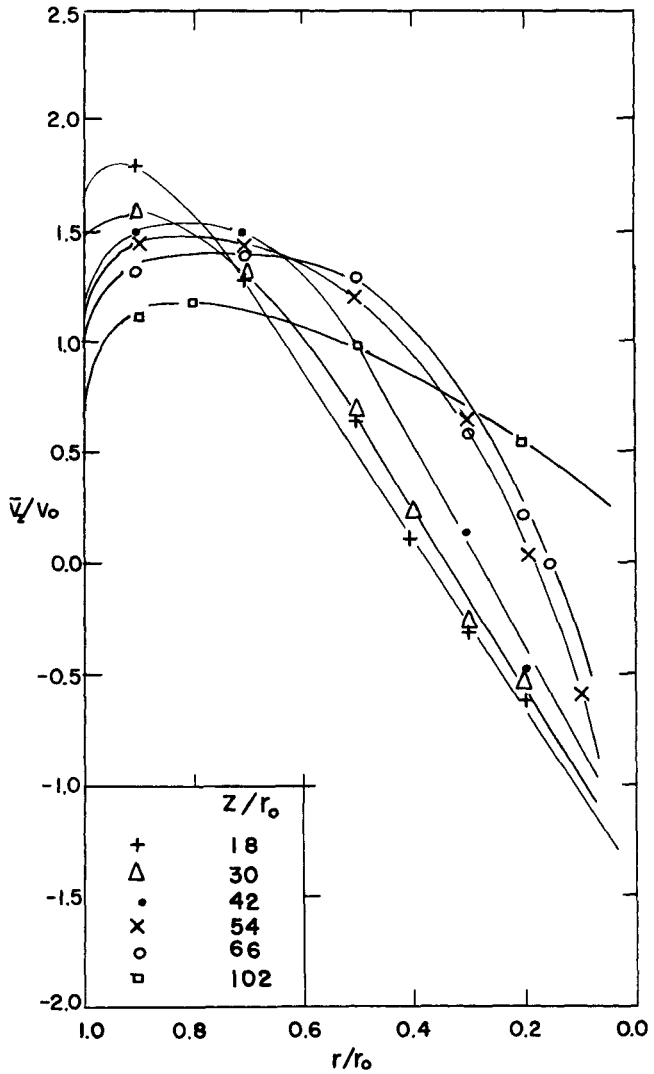

Fig. 5. Dimensionless axial velocity profiles (N_{Re0} = 15,000).

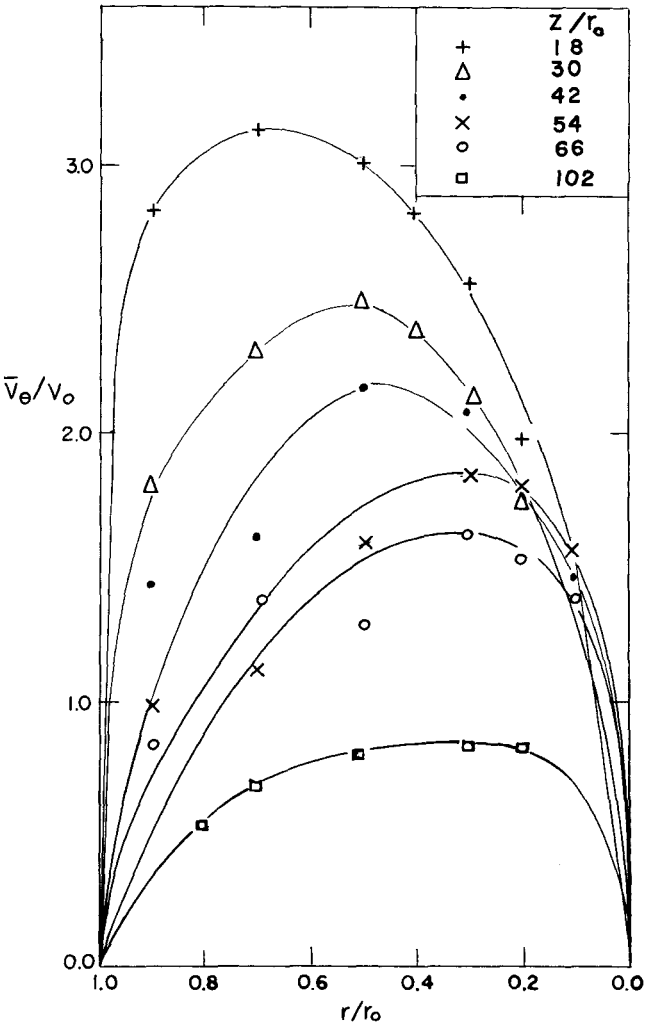

Fig. 6. Dimensionless tangential velocity profiles (N_{Re0} = 15,000).

The angle of flow was then used to resolve $\overline{v}/v_0$ into $\overline{v}_z/v_0$ and $\overline{v}_\theta/v_0$, the dimensionless axial and tangential velocities.

RESULTS AND DISCUSSION

Dimensionless static pressure, axial velocity, and tangential velocity profiles were obtained at z/r_0 = 18, 30, 54, and 102 for N_{Re0} = 10,000, 15,000, 20,000, and 25,000, and additionally at z/r_0 = 42 and 66 for N_{Re0} = 15,000. The profiles obtained at N_{Re0} = 15,000 are presented in Figures 5 to 7. Profiles measured at the other Reynold's numbers are quite similar. As may be seen from Figure 5, at small z/r_0, the axial velocity rises quickly from zero at the tube wall to a maximum value at an r/r_0 of about 0.9. It then decreases, passes through $\overline{v}_z/v_0 = 0$, and continues to drop as the centerline is approached. (Measurements were not made at the centerline since the probes were found to give very erratic readings as the distance from the centerline approached the probe hole size.) At higher z/r_0, the maximum $\overline{v}_z/v_0$ decreases and moves in further toward the centerline. In addition, the r/r_0 at which $\overline{v}_z/v_0 = 0$ decreases and finally becomes zero (no reverse flow).

From Figure 6, the tangential velocity rises from zero at the wall to a maximum between the wall and centerline and drops off again to zero at the centerline. As may be seen, the value of the maximum $\overline{v}_\theta/v_0$ and the r/r_0 at which it occurs both decrease with increasing z/r_0. The flow pattern may be considered to be a nonideal free vortex above this maximizing r/r_0 and a nonideal forced vortex for smaller r/r_0. Thus, with increasing z/r_0, the

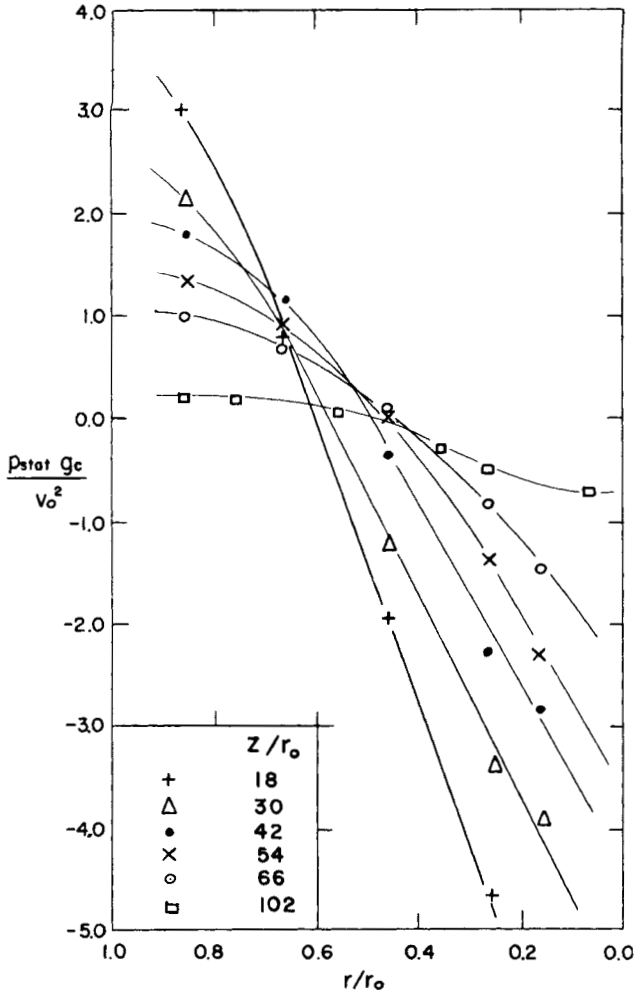

Fig. 7. Dimensionless static pressure profiles ($N_{Re_0} = 15{,}000$).

initial forced vortex may be considered to decay partially into a free vortex while the total vorticity is decreased by friction. Though there is some indication of a plateau region of $\overline{V}_\theta/V_0$ vs. r/r_0 at stations 3 and 4, it is not felt that the data is accurate enough to justify such a conclusion or drawing of the curves in such a manner, in addition, such a plateau is not indicated in data taken at the other values of N_{Re_0}. A good measure of the decay of swirl in that test section is provided by a plot of the weighted tangential velocity to inlet velocity ratio vs. z/r_0. The weighted tangential velocity $\overline{\overline{v}}_\theta$ is defined by $\overline{\overline{v}}_\theta = (\int_0^{r_0} 2\pi\, r\bar{v}_\theta\, dr)/\pi r_0^2$. Decay curves are presented in Figure 8.

As would be expected, Figure 7 indicates that the static pressure at a given z/r_0 increases monotonically from the centerline to the wall. With increasing z/r_0, the magnitude of this gradient decreases as the gradient producing swirl decays. In addition, it is particularly interesting to note that at, and near, the centerline the axial pressure gradient is positive for considerable distance from the tube.

To explain flow reversal phenomena occurring in unconfined vortex flows, Brooke-Benjamen (2) has developed a very interesting theory postulated on the existence of a super critical flow regime whose breakdown leads to the flow reversal. This treatment is developed along line analogous to hydraulic jump theory and may well be the proper explanation for unconfined flows where boundary layer effects do not enter. However, in the system studied in this work, boundary layer effects are obviously quite large and provide another logical explanation for the flow reversal based on the decay of the initially very strong vortex by wall friction. First, the existence of a very strong swirl near the end of the tube leads to a large pressure differential across the tube cross section, centerline static pressure being considerably lower than wall static pressure. Further downstream, where the swirl has been dissipated to a large extent by friction, the pressure gradient from the centerline to wall is considerably less. Thus, it is possible for the axial pressure gradient along the centerline to be positive while the wall gradient is negative, and the positive pressure gradient along the centerline may then serve to drive fluid along the centerline back toward the head-end of the tube (flow reversal).

In further reference to the Brooke-Benjamen model, discontinuities in flow variables are required at the point of the vortex breakdown as the flow changes from one conjugate state to the other (analogous to the change in properties across a shock in compressible flow). However, the measurements made in this work indicate continuous velocities, pressures, and first derivatives of each throughout the flow studied, thus lending support to the postulated smooth frictional vortex decay mechanism described above.

Bresan (*4, 9*) has presented a frictional vortex decay model predicting where reverse flow will occur in the type of system studied here. The basis of his model is the assumption that $\bar{v}_z < 0$ (reverse flow) wherever $\partial\bar{p}/\partial z > 0$ and that $\bar{v}_z > 0$ wherever $\partial\bar{p}/\partial z < 0$ (that is, no flow against a pressure gradient). However, such an assumption is not necessarily true for a multidimensional flow system. Indeed, the data taken by this author show that there is a region in this system where $\partial\bar{p}/\partial z > 0$ and $\bar{v}_z > 0$ (flow against a pressure gradient). In Figure 9, the line separating the regions where $\partial\bar{p}/\partial z > 0$ and $\partial\bar{p}/\partial z < 0$, and the line separating the regions where $\bar{v}_z > 0$ and $\bar{v}_z < 0$ for $N_{Re_0} = 15{,}000$ are plotted. If Bresan's assumption were correct, these lines would be identical. However, it may be seen that there exists an annular conical region in which $\bar{v}_z > 0$ and $\partial\bar{p}/\partial z > 0$. This region also appears at the other Reynold's numbers investigated.

In addition, when Bresan's own data (Figure 10) for his very similar system are analyzed in this manner, this same type of region is found. Therefore, though his model may be useful for predicting the sign of $\partial\bar{p}/\partial z$ at a given point, it is not adequate for predicting whether or not the axial flow is reversed at that point.

An explanation for the existence of this region of flow against the axial pressure gradient may be developed from careful examination of the axial Navier-Stokes equation

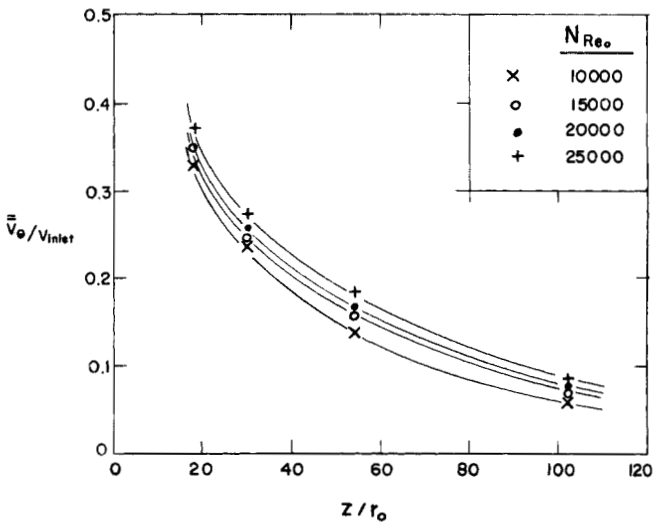

Fig. 8. Vortex decay curves.

(simplified by discarding of negligible terms) along with velocity and velocity gradient data obtained during this study.

$$-\frac{\partial p}{\partial z} = \rho\, v_z \frac{\partial v_z}{\partial z} + \rho\, v_r \frac{\partial v_z}{\partial r} - \frac{(\mu+\epsilon)}{r}\,\frac{\partial}{\partial r}\left(r\frac{\partial v_z}{\partial r}\right) \tag{5}$$

Examination of Figure 5 shows that over most of the flow (and particularly in the region of interest) $\partial v_z/\partial r > 0$, $\simeq$ constant. In addition, solution for v_r from the equation of continuity [Equation (4)] indicates that in the region of interest, v_r is usually less than zero. Thus,

$$\frac{-\partial p}{\partial z} < \rho\, v_z \frac{\partial v_z}{\partial z} \tag{6}$$

from which it may be concluded that at the boundary defined by $v_z = 0$, $\partial p/\partial z > 0$ as is indeed observed. That is, the radial transport of axial momentum, both by convection and shear forces leads to the existence of the region of flow against the axial pressure gradient.

As mentioned earlier, the equations of motion describing this system of swirling flow with strong dissipative effects are quite complex (and, in fact, are indeterminate due to the presence of turbulent shear stress terms). An approach which appears to be useful in simplifying them to some extent is an order of magnitude analysis using the data taken in this study. The turbulent Navier-Stokes equations for this system can be written in dimensionless form (neglecting viscous stresses as compared to turbulent stresses) as follows:

$$\left[(v_r/v_0)\frac{\partial(\bar{v}_r/v_0)}{\partial(r/r_0)} - \frac{(\bar{v}_\theta/v_0)^2}{(r/r_0)} + (\bar{v}_z/v_0)\frac{\partial(\bar{v}_r/v_0)}{\partial(z/r_0)} \right] = -\frac{\partial(\bar{p}g_c/v_0^2)}{\partial(r/r_0)} - \left[\frac{r_0}{r}\frac{\partial(r/r_0\overline{v_r'/v_0 v_r'/v_0})}{\partial(r/r_0)} + \frac{\partial(\overline{v_r'/v_0 v_z'/v_0})}{\partial(z/r_0)} - \frac{\overline{v_\theta'/v_0 v_\theta'/v_0}}{r/r_0} \right] \tag{7}$$

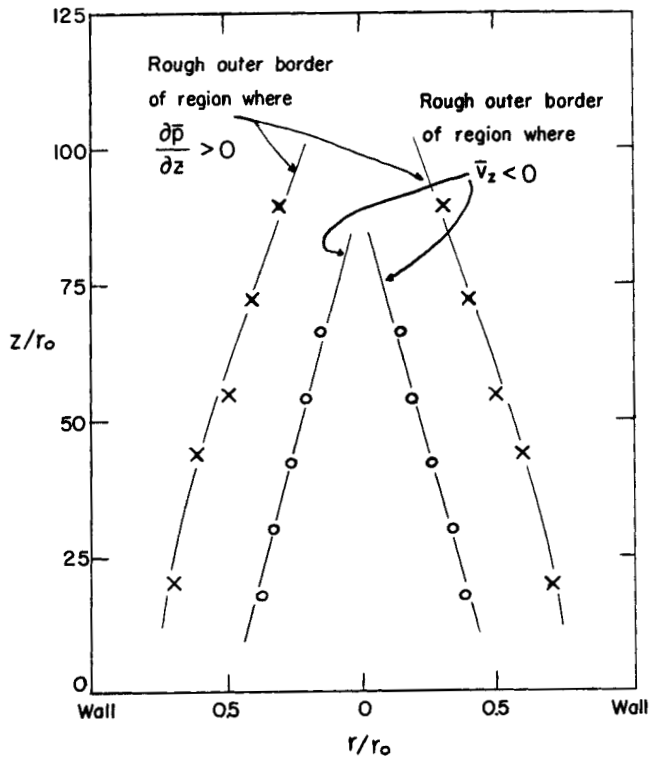

Fig. 9. Transition regions in test section ($N_{Re_0} = 15{,}000$).

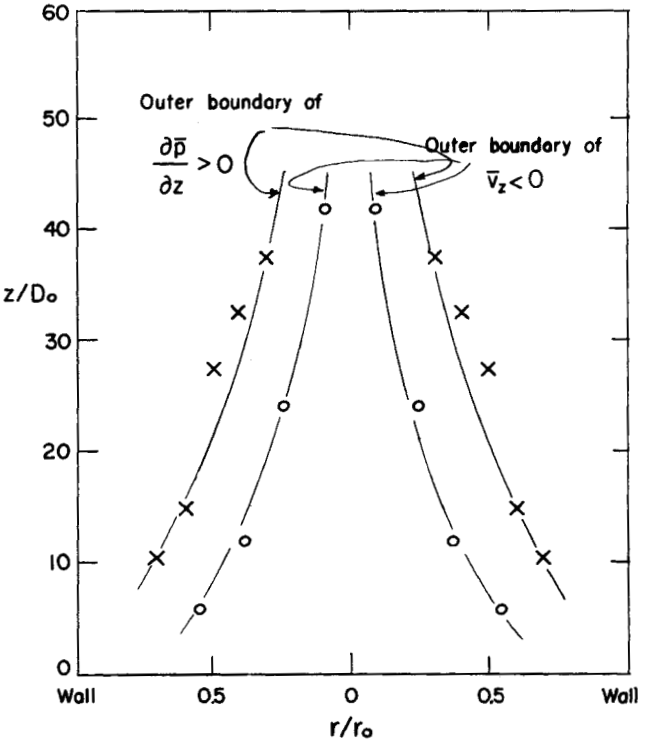

Fig. 10. Transition regions in test section for Breasan's data ($N_{Re_0} =$ 15,000).

$$\left[(\bar{v}_r/v_0)\frac{\partial(\bar{v}_\theta/v_0)}{\partial(r/r_0)} + \frac{(\bar{v}_\theta/v_0)(\bar{v}_r/v_0)}{r/r_0} + (\bar{v}_z/v_0)\frac{\partial(\bar{v}_\theta/v_0)}{\partial(z/r_0)} \right] = -\left[(r_0/r)^2 \frac{\partial(r^2/r_0^2\overline{v_r'/v_0 v_\theta'/v_0})}{\partial(r/r_0)} + \frac{\partial(\overline{v_z'/v_0 v_\theta'/v_0})}{\partial(z/r_0)} \right] \tag{8}$$

$$\left[(\bar{v}_r/v_0)\frac{\partial(\bar{v}_z/v_0)}{\partial(r/r_0)} + (\bar{v}_z/v_0)\frac{\partial(\bar{v}_z/v_0)}{\partial(z/r_0)} \right] = -\frac{\partial(\bar{p}g_c/v_0^2)}{\partial(z/r_0)} - \left[(r_0/r)\frac{\partial(r/r_0\overline{v_r'/v_0 v_z'/v_0})}{\partial(r/r_0)} + \frac{\partial(\overline{v_z'/v_0 v_z'/v_0})}{\partial(z/r_0)} \right] \tag{9}$$

$$(r_0/r)\frac{\partial(r/r_0\bar{v}_r/v_0)}{\partial(r/r_0)} + \frac{\partial(\bar{v}_z/v_0)}{\partial(z/r_0)} = 0 \tag{10}$$

From the system definition:

$$r/r_0 \simeq 0(1)$$

$$v_z/v_0 \simeq 0(1)$$

In addition, $\Delta(r/r_0)$ may be so picked that

$$\partial/\partial(r/r_0) \simeq 0(1)$$

By definitions

$$\partial/\partial(z/r_0) \simeq 0(\delta)$$

$$\bar{v}_r/v_0 \simeq 0(\epsilon)$$

$$\frac{\overline{v_r'v_r'}}{v_0^2}, \frac{\overline{v_z'v_z'}}{v_0^2}, \frac{\overline{v_z'v_\theta'}}{v_0^2}, \text{ etc.}, \simeq 0(\beta)$$

$$\bar{v}_\theta/v_0 \simeq 0(\eta)$$

$$\partial(\bar{p}g_c/v_0^2) \simeq 0(\gamma)$$

From analysis of the data at $N_{Re0} = 15{,}000$, (these data were used since they were most complete) estimates of δ, ϵ, β, η, and γ were obtained.

$$\epsilon \simeq \delta \simeq 1/200$$

$$\beta \simeq 1/25$$

$$\gamma \simeq 4$$

$$\eta \simeq 2$$

These values were substituted into Equations (7), (8), and (9) to see which terms in these equations could be discarded. This analysis follows:

Equation (7)

1st term:	0(1/200) 0(1/200)	negligible
2nd term:	0(4)	
3rd term:	0(1) 0(1/200) 0(1/200)	negligible
4th term:	0(4)	
5th term:	0(1/25)	
6th term:	0(1/25) 0(1/200)	negligible
7th term:	0(1/25)	

Terms 5 and 7 are each only $\simeq 1/100$ of terms 2 and 4. Therefore:

$$\frac{(\bar{v}_\theta/v_0)}{r/r_0} = \frac{\partial(\bar{p}g_c/v_0^2)}{\partial(r/r_0)} + 0(2\%),\ 5 \text{ terms rejected}$$

Equation (8)

1st term:	0(1/200)	
2nd term:	0(1/200) 0(2)	
3rd term:	0(1/200) 0(2)	
4th term:	0(1/25)	
5th term:	0(1/25) 0(1/200)	negligible

Therefore:

$$(\bar{v}_r/v_0)\frac{\partial(v_\theta/v_0)}{\partial(r/r_0)} + \frac{(\bar{v}_\theta/v_0)(\bar{v}_r/v_0)}{r/r_0} + (\bar{v}_z/v_0)\frac{\partial(\bar{v}_\theta/v_0)}{(z/r_0)} = -\frac{r_0^2}{r^2}\left(\frac{\partial(r^2/r_0^2\overline{v_r'/v_0 v_\theta'/v_0})}{\partial(r/r_0)}\right) + 0(4\%),\ 1 \text{ term rejected}$$

Equation (9)

1st term:	0(1/200)	
2nd term:	0(1/200)	
3rd term:	0(4) 0(1/200)	
4th term:	0(1/25)	
5th term:	0(1/25) 0(1/200)	negligible

$$(\bar{v}_z/v_0)\frac{\partial(\bar{v}_z/v_0)}{\partial(z/r_0)} + (\bar{v}_r/v_0)\frac{\partial(\bar{v}_z/v_0)}{\partial(r/r_0)} = -\frac{\partial(\bar{p}g_c/v_0^2)}{\partial(z/r_0)} - \frac{r_0}{r}\frac{\partial(r/r_0\overline{v_r'/v_0 v_z'/v_0})}{\partial(r/r_0)} + 0(4\%),\ 1 \text{ term rejected.}$$

SUMMARY OF RESULTS

1. Dimensionless static pressure, axial velocity, and tangential velocity profiles were developed for the system. It was found that the flow could be roughly divided into free and forced vortex regions. With increasing z/r_0, the initial forced vortex decayed into a free vortex while overall the total vorticity was decreased by friction. A region of reverse axial flow was noted in the center of the tube, the radius of this region decreasing with increasing z/r_0 to zero.

2. Curves of the weighted tangential velocity/inlet velocity vs. z/r_0 were developed as a form of representation of the swirl decay.

3. Contrary to a previously proposed model, it was found that there exists a conical annular region in the system in which $\bar{v}_z > 0$ and $\partial\bar{p}/\partial z > 0$, that is, a region of flow against a pressure gradient.

4. The turbulent Navier-Stokes equations were simplified to some extent, even though the simplified set was still indeterminate due to the presence of turbulent shear stress terms, by an order of magnitude analysis using the profiles developed in this study.

NOTATION

D_0 = test section tube diameter
g_c = 32.2 lb.$_m$/lb.$_f$ ft./sq.sec.
$p = p_{stat}$ = static pressure
p_{stag} = stagnation pressure
r = radial distance
r_0 = test section tube radius
N_{Re0} = Reynold's number = $D_0 v_0 \rho/\mu$
v_0 = average axial velocity in test section (vol. flow rate/area)
v_θ = instantaneous local tangential (circumferential) velocity
v_z = instantaneous local axial velocity
v_r = instantaneous local radial velocity
v_{inlet} = average velocity in inlet tube
z = axial distance down main tube, referred from inlet plane
ρ = density
μ = viscosity
θ = angular coordinate in test section
τ_{ij} = shear stress in j-direction exerted on surface of constant i
overscore = temporal mean value of quantity
prime = fluctuating component of quantity

LITERATURE CITED

1. Beal, G. F., Unpublished research, Carnegie Mellon Univ., Pittsburgh, Pa. (1962).
2. Benjamin, T. Brooke, *J. Fluid Mech.*, **14**, 593 (1962).
3. Binnie, A. M., *Quart. J. Mech. Appl. Math.*, **30**, No. 3, 276 (1957).
4. Bresan, V. P., Ph.D. thesis, Rensselaer Polytechnic Inst., Troy, N. Y. (1960).
5. Deissler, R. G., and M. Perlmutter, *Int. J. Heat Mass Transfer*, **1**, No. 2, 3, 173 (Aug., 1960).
6. King, M. K., Ph.D. thesis, Carnegie Mellon Univ., Pittsburgh, Pa. (1964).
7. Kreith, F. and O. K. Sonju, *J. Fluid Mech.*, **22**, 257 (1965).
8. Lay, *J. Heat Transfer*, 202 (Aug., 1959).
9. Nissan, A. F., and V. P. Bresan, *AIChE J.*, **7**, 543 (1961).
10. Nuttall, J. B., *Nature*, **172**, 582 (Sept. 26, 1953).
11. Peck, D. F., Unpublished senior project, Carnegie Mellon Univ., Pittsburgh, Pa.
12. Scheller, W. A., and G. M. Brown, *Ind. Eng. Chem.*, **49**, No. 6, 1013 (June, 1957).
13. Sibulkin, M., *J. Fluid Mech.*, **12**, 269 (Feb., 1962).
14. Suzuki, M., *Inst. Phys. Chem. Res. (Tokyo)*, **54**, 1, 42 (Mar., 1960).
15. Talbot, L., *J. Appl. Mech.*, **21**, 1 (1954).

Manuscript received April 24, 1967; revision received April 29, 1968; paper accepted May 1, 1968.